BBA - Bioenergetics 1860 (2019) 136–146

Contents lists available at ScienceDirect

BBA - Bioenergetics

journal homepage: www.elsevier.com/locate/bbabio

Photochemical study of a cyanobacterial chloride-ion pumping rhodopsin

Takatoshi Hasemi[a], Takashi Kikukawa[a,b,*], Yumi Watanabe[a], Tomoyasu Aizawa[a,b], Seiji Miyauchi[c], Naoki Kamo[a], Makoto Demura[a,b]

[a] Faculty of Advanced Life Science, Hokkaido University, Sapporo 060-0810, Japan
[b] Global Station for Soft Matter, Global Institution for Collaborative Research and Education, Hokkaido University, Sapporo 060-0810, Japan
[c] Graduate School of Pharmaceutical Sciences, Toho University, Chiba 274-8510, Japan

ARTICLE INFO

Keywords:
Halorhodopsin
Light-driven chloride pump
Photocycle
Flash photolysis
Microbial rhodopsin

ABSTRACT

Mastigocladopsis repens halorhodopsin (MrHR) is a Cl^--pumping rhodopsin that belongs to a distinct cluster far from other Cl^- pumps. We investigated its pumping function by analyzing its photocycle and the effect of amino acid replacements. MrHR can bind I^- similar to Cl^- but cannot transport it. I^--bound MrHR undergoes a photocycle but lacks the intermediates after L, suggesting that, in the Cl^--pumping photocycle, Cl^- moves to the cytoplasmic (CP) channel during L decay. A photocycle similar to that of the I^--bound form was also observed for a mutant of the Asp200 residue, which is superconserved and assumed to be deprotonated in most microbial rhodopsins. This residue is probably close to the Cl^--binding site and the protonated Schiff base, in which a chromophore retinal binds to a specific Lys residue. However, the D200N mutation affected neither the Cl^--binding affinity nor the absorption spectrum, but completely eliminated the Cl^--pumping function. Thus, the Asp200 residue probably protonates in the dark state but deprotonates during the photocycle. Indeed, a H^+ release was detected for photolyzed MrHR by using an indium-tin oxide electrode, which acts as a good time-resolved pH sensor. This H^+ release disappeared in the I^--bound form of the wild-type and Cl^--bound form of the D200N mutant. Thus, Asp200 residue probably deprotonates during L decay and then drives the Cl^- movement to the CP channel.

1. Introduction

Many organisms express photoactive proteins to utilize sunlight as an information and energy source. Microbial rhodopsins are the most ubiquitous photoactive proteins and are present in the cell membranes of unicellular microorganisms [1,2]. Like visual rhodopsins, they utilize the photoisomerization of retinal chromophores to trigger sequential changes in protein conformation. However, the resultant functions are not confined to light sensors. They also function as light-driven ion pumps, light-gated ion channels, and even as light-switchable enzymes. Among these, ion-pumping rhodopsins are the most abundant in the microbial world.

The first and second identified ion pumps were outward H^+ pump bacteriorhodopsin (BR) [3] and inward Cl^- pump halorhodopsin (HR) [4,5]. They were discovered in halophilic archaea in the 1970s and proven to play roles in light-driven ATP production [6,7]. For HR, its Cl^- transport is also believed to maintain a cellular osmotic balance during the volume increases of growing cells [8]. Since 2000, various ion pumps have been identified in other microorganisms. In particular, many representatives were found among marine bacteria: outward H^+ pump proteorhodopsin (PR) [9], outward Na^+ pump *Krokinobacter eikastus* rhodopsin 2 (KR2) [10] and inward Cl^- pump *Nonlabens marinus* rhodopsin 3 (NM-R3) [11]. All ion pumps have essentially identical structural folds and show the photoinduced conformational changes due to their common retinal isomerization from all-*trans* to 13-*cis*. Thus, their functional differences are probably caused by differences among residues at key positions. In particular, three residues on the C-helix (the third helix) are considered important. For BR, they are Asp85, Thr89 and Asp96 and thus are designated the DTD motif. The corresponding residues are TSA for HR, DTE for PR, NDQ for KR2, and NTQ for NM-R3.

Recently, we found a new class of microbial rhodopsin from

Abbreviations: BR, bacteriorhodopsin; HR, halorhodopsin; PR, proteorhodopsin; KR2, *Krokinobacter eikastus* rhodopsin 2; NM-R3, *Nonlabens marinus* rhodopsin 3; MrHR, *Mastigocladopsis repens* halorhodopsin; SyHR, rhodopsin from *Synechocystis* sp. PCC7509; EC, extracellular; CP, cytoplasmic; ITO, indium-tin oxide; NpHR, HR from *Natronomonas pharaonis*; SRII, sensory rhodopsin II; K_d, dissociation constant of Cl^-; DDM, *n*-dodecyl-β-D-maltopyranoside; CCCP, carbonyl cyanide *m*-chlorophenylhydrazone; PC, phosphatidylcholine; HsHR, HR from *H. salinarum*

* Corresponding author at: Faculty of Advanced Life Science, Hokkaido University, N10W8, Kita-ku, Sapporo 060-0810, Japan.
E-mail address: kikukawa@sci.hokudai.ac.jp (T. Kikukawa).

https://doi.org/10.1016/j.bbabio.2018.12.001
Received 31 August 2018; Received in revised form 30 November 2018; Accepted 4 December 2018
Available online 07 December 2018

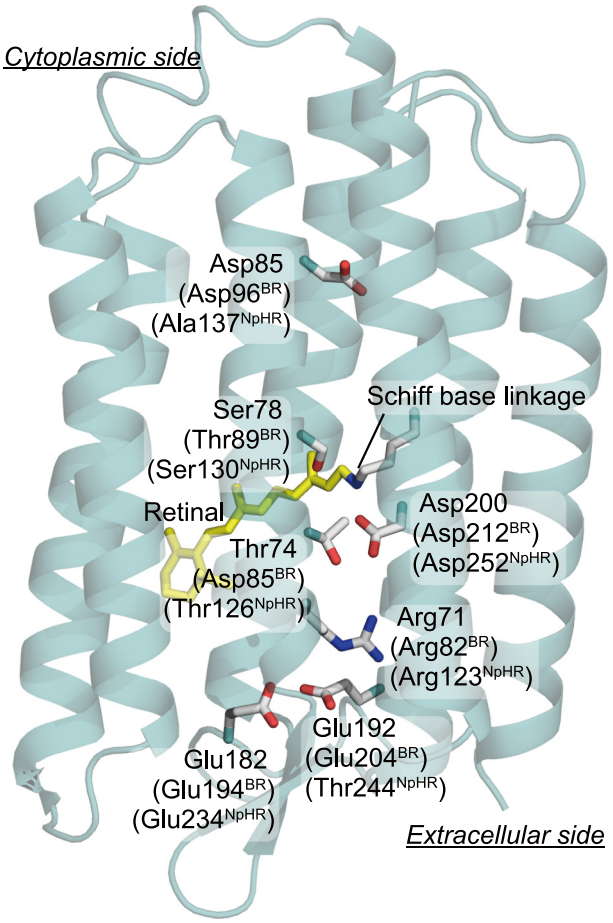

Fig. 1. Putative positions of the residues of MrHR. The MrHR structure is modeled from the SwissModel server using the BR (PDB code: 1C3W) as a template. The corresponding residues in BR and NpHR are indicated in parentheses.

cyanobacteria and functionally characterized one member from the cyanobacterium *Mastigocladopsis repens* [12]. This rhodopsin was designated *M. repens* HR (MrHR) because its Cl^--pumping function is same as that of the archaeal HR. Actually, MrHR homologs conserve the TSD motif, which is close to the TSA in HR despite their low amino acid identity (22%). From this TSD group, a unique rhodopsin was also reported: a rhodopsin from *Synechocystis* sp. PCC7509 (SyHR) was revealed to pump not only Cl^- but also SO_4^{2-} [13]. The latter ion is never pumped by archaeal HR. Despite their anion pumping abilities, MrHR homologs highly conserve key residues for the H^+ pump BR [12]. Notably, they conserve the third "D" residue in the BR motif (DTD for BR, TSD for MrHR). These residues are Asp96 for BR and Asp85 for MrHR (Fig. 1). In the photolyzed BR, the H^+ of the Schiff base first moves to another "D" residue (Asp85 of BR) in the extracellular (EC) channel. This H^+ acceptor corresponds to the first "D" residue in the BR motif (DTD). The deprotonated Schiff base subsequently captures another H^+ from the cytoplasmic (CP) medium. The third "D" residue significantly accelerates this reaction, in which the "D" residue first donates H^+ to the Schiff base and then captures another H^+ from the CP medium. In addition to the third "D" residue, many MrHR homologs also conserve two Glu residues corresponding to Glu194 and Glu204 of BR; they are Glu182 and Glu192 for MrHR, respectively (Fig. 1). In BR, these Glu residues act as H^+ releasing complex to EC media and contribute to a high H^+ pumping activity [14,15]. Thus, MrHR homologs have conserved the residues that are characteristic for both the Cl^- pump HR and the H^+ pump BR. Indeed, we previously proved that MrHR converts into an outward H^+ pump by only the introduction of the H^+ acceptor Asp residue, which corresponds to the first "D" residue in the BR motif [12]. In this T74D mutant of MrHR, the third "D" residue (Asp85 of MrHR) functions well, as does the corresponding Asp96 residue of BR. These observations suggest that MrHR evolved from the BR-type H^+ pump and acquired a Cl^--pumping ability owing to the TSD motif but has not been fully optimized compared with other Cl^- pumps.

In this work, we aimed to understand the molecular differences of MrHR from other Cl^- pumps, especially HR. The analyses using various mutants revealed several characteristic features of MrHR. In particular, protonation state of Asp200 (corresponding to Asp212 of BR) is notable. Different from other microbial rhodopsins, this Asp residue is probably protonated in the dark state but deprotonates during the photocycle. The resultant negative charge appears to be prerequisite for the Cl^- movement to the CP channel. Based on these results, we will discuss the differences between MrHR and other Cl^- pumps.

2. Materials and methods

2.1. Expression and purification of MrHR

Escherichia coli strain DH5α was used for the DNA manipulation. The construction of the expression plasmid of a six-histidine tagged MrHR was described previously [12]. The mutations were introduced using the Quikchange site-directed mutagenesis kit (Agilent Technologies, Santa Clara, CA), and the sequences were confirmed by a standard method using an automated DNA sequencer (model 3100, Applied Biosystems, Foster City, CA). MrHR and the mutants were expressed and purified from *E. coli* strain BL21(DE3) as previously described [12]. The purified samples were placed into appropriate buffer solutions by passage over Sephadex G-25 in a PD-10 column (Amersham Bioscience, Uppsala Sweden).

2.2. Preparation of archaeal HR and the mutant

The wild-type HR from *Natronomonas pharaonis* (NpHR) and its D252N mutant were expressed in *Halobacterium salinarum*. First, we prepared their pET plasmids (Novagen). The construction of pET-NpHR was described elsewhere [16]. The mutation for D252N was introduced using the same method as for the MrHR mutants described above. The expression plasmids for *H. salinarum* were constructed by modification of the pJS010 plasmid as described previously [17]. The obtained plasmids were introduced into the *H. salinarum* strain Pho81Wr$^-$ [18], and the transformants were grown in the presence of 4 μM mevinolin. The membrane fragments containing the expressed NpHR and the D252N were prepared as described previously [19].

2.3. Absorption spectrum measurements

The absorption spectra of unphotolyzed MrHR and NpHR were measured by a UV1800 spectrometer (Shimadzu, Kyoto, Japan). All measurements were performed at room temperature. The Cl^--induced spectral changes were analyzed by the following two Hill equations independently:

$$\Delta A = \Delta A_{max} \frac{[Cl^-]^n}{K_d{}^n + [Cl^-]^n} \quad (1)$$

$$\lambda_{max} = \Delta\lambda_{max} \frac{[Cl^-]^n}{K_d{}^n + [Cl^-]^n} + \lambda_{max,0} \quad (2)$$

where the absorbance changes (ΔA) at specific wavelengths and the Cl^--induced λ_{max} shifts were analyzed, respectively. The common parameters of K_d, n and $[Cl^-]$ represent dissociation constant, Hill coefficient, and Cl^- concentration, and other parameters of ΔA_{max}, $\Delta\lambda_{max}$ and $\lambda_{max,0}$ represent the maximum absorbance change, the shift width of λ_{max}, and the λ_{max} in the Cl^- free state, respectively. The

spectra of MrHR were measured in the *n*-dodecyl-β-D-maltopyranoside (DDM) solubilized state, while those of NpHR were measured in the membrane fragments isolated from *H. salinarum* cells. These fragments are easily aggregated in the presence of a high salt concentration. Thus, we encased them within 15% acrylamide gel after suspending them in 0.1 M NaCl. The obtained gels were soaked in the buffer solutions containing various concentrations of Cl^- and then used for spectral measurements.

2.4. Flash photolysis spectroscopy

The flash photolysis apparatus equipped with a Nd-YAG laser (532 nm, 7 ns) was described previously [20]. To improve the S/N ratio, 30 laser pulses were used at each measurement wavelength. The temperature was maintained at 25 °C for all measurements. Data points on a logarithmic time scale were picked from the observed data for plots and for the following analysis. The datasets, measured at 400–700 nm with a 10 nm interval, were analyzed based on an irreversible sequential model: $P_0 \rightarrow P_1 \rightarrow P_2 \rightarrow \ldots \rightarrow P_i \rightarrow P_0$, where P_0 represents the original unphotolyzed state and P_i represents the *i*th photochemically defined state [21]. This model contains only forward reactions between the P_i states. Thus, these P_i states may contain a few physically defined intermediates when the reverse reactions exist between them. The details of this procedure were described previously [22]. Briefly, the data were fitted by multi-exponential functions simultaneously for a data set of all wavelengths. The appropriate number of exponents (*i*) was determined from the reduction in the standard deviation of weighted residuals. Using the fitting results, the time constants τ_i and the absorption differences between P_i and P_0 ($\Delta\varepsilon_i$) were calculated. Independently, the P_0 spectrum was obtained by subtracting the background scattering ($A + B/\lambda^4$; λ in nanometer) from the measured spectrum of the unphotolyzed state in 4 M NaCl. Here, the second term "B/λ^4" of the above equation reflects that the intensity of Rayleigh light scattering is proportional to $1/\lambda^4$. Finally, absolute spectra of P_i states were obtained by adding the spectrum of P_0 to the absorption differences, $\Delta\varepsilon_i$.

Several microbial rhodopsins are reported to have branched pathways at the end of their photocycles [23–25]. For such branched photocycles, it is challenging to apply the unbranched scheme described above, because the P_i states should become complex mixtures of several intermediates reflecting the branching efficiency and respective kinetic constants. Thus, further analysis is necessary to fully describe such branched reactions as demonstrated for NpHR [24]. However, the present analysis is still useful to know the absorption spectra and appearance timings of the intermediates, which are important clues to understand the photocycle outline.

2.5. Chloride ion pump activity measurement

The ion-pumping activities of MrHR and the mutants were measured in *E. coli* suspensions using a conventional pH electrode method, which detects light-induced alkalization by passive H^+ transfer in response to the membrane potential by the Cl^--pump activity. The experimental details were slightly modified from the previously reported technique [12]. Briefly, the cells expressing MrHR were harvested and washed twice with a 200 mM NaCl solution. After overnight shaking in the presence of 10 μM carbonyl cyanide *m*-chlorophenylhydrazone (CCCP), the cells were washed twice and finally suspended in the same salt solution at an A_{660} of 2.0. The sample volume was 10 mL. Before the measurements, 10 μM CCCP was added to the sample cuvette. For the activation of MrHR, 530 ± 17.5 nm of green LED light (LXHL-LM5C, Philips Lumileds Lighting Co., San Jose, CA) was used. All measurements were performed at room temperature, which was approximately 25 °C.

The ion pumping activities depend on the expression levels of MrHR. Thus, those levels were estimated from independent experiments. After the ion-pumping activity measurements, the cells were centrifuged and then suspended in 2 mL of 50 mM MES, pH 6, containing 0.2 M NaCl. The cells were disrupted with sonication. The resultant lysates were used for measurements of flash-induced absorbance changes. The measuring wavelengths were set to the respective λ_{max} values of the wild-type MrHR and the mutants. The flash-induced signals reached their maxima approximately 0.1–2 ms. These maximum values (ΔA_{max}) were used for the relative amounts of the expressed MrHR. The relative ion pumping activities were calculated by dividing the initial slopes of the light-induced pH changes with ΔA_{max}.

2.6. Measurements of photoinduced proton transfer reactions

The flash-induced H^+ transfers were measured by using the ITO electrode, which acts as a time-resolved pH sensor [26]. For these measurements, the purified MrHR samples were reconstituted with phosphatidylcholine (PC) from egg yolk (Avanti, Alabaster, AL, USA) at an MrHR:PC molar ratio of 1:30 as described previously [27]. The reconstituted sample was suspended in distilled water with a protein concentration of ~10 μM under an assumed molar extinction coefficient of 40,000 $M^{-1}\,cm^{-1}$ at the respective λ_{max}. The suspension of 100 μL was applied to the surface of an ITO electrode, followed by the evaporation of water under reduced pressure to produce a dried film. This electrode was placed into the electrochemical cell, in which a buffer solution was sandwiched with another "bare" ITO electrode. The buffer solution was the 6 mix buffer (1.37 mM citric acid, 0.46 mM ADA, 1.04 mM MOPS, 1.25 mM TAPS, 0.81 mM CHES, 1.39 mM CAPS) containing 0.1 M NaCl or 0.1 M NaI. The samples were excited by a 7 ns laser pulse (532 nm, 0.6 mJ/pulse) from a Q-switched Nd:YAG laser (Minilite I, Continuum, San Jose, CA, USA). The electric signal from the ITO electrodes was recorded after amplification. To improve the S/N ratio, 60 laser pulses were used. All measurements were performed at room temperature, which was approximately 25 °C. The details of the apparatus have been reported elsewhere [28].

3. Results and discussion

3.1. Photocycles of the Cl^--bound and I^--bound forms

Similar to other Cl^- pumps, unphotolyzed MrHR readily binds to the substrate Cl^- [12]. This can be detected by the Cl^- induced shift of the retinal absorption spectrum in the dark. From analogies with other Cl^- pumps, the binding site should be close to the Schiff base NH^+ facing toward the EC sides. Upon illumination, this Cl^- probably moves to the CP channel and is then released into the CP medium. In addition to Cl^-, other Cl^--pumping rhodopsins can transport Br^- and I^- [29–31]. MrHR can also bind Br^- and I^- but cannot transport I^-, suggesting that MrHR cannot move I^- to the CP channel over the Schiff base region [12]. Thus, the photocycle of I^--bound MrHR probably lacks the intermediates after this Cl^- movement. To examine this assumption, we compared the photocycles of the Cl^-- and I^--bound forms.

Fig. 2 shows the flash-induced absorbance changes with 1 M Cl^- (left column) and 1 M I^- (right column). The top panels show the time-dependent absorbance changes at typical wavelengths, and the lower panels are the light-dark difference spectra divided into three time regions, which are denoted I-III for the Cl^--bound form and I′–III′ for the I^--bound form. Previously, we named the intermediates of MrHR referring to the photocycle with 0.1 M Cl^- [12]. The same intermediates were also observed here. MrHR has an absorption maximum at approximately 540 nm in both the Cl^--bound and the I^--bound forms. Thus, the negative deflections due to flash excitation reach a maximum at approximately 540 nm. Within time region I (Panels A and B), the negative band at approximately 540 nm further develops without a peak shift. This reflects the decay of K. No peak shift indicates a nearly identical λ_{max} between the K and the original dark state. Concomitant with the K decay, the band at approximately 460 nm slightly increases

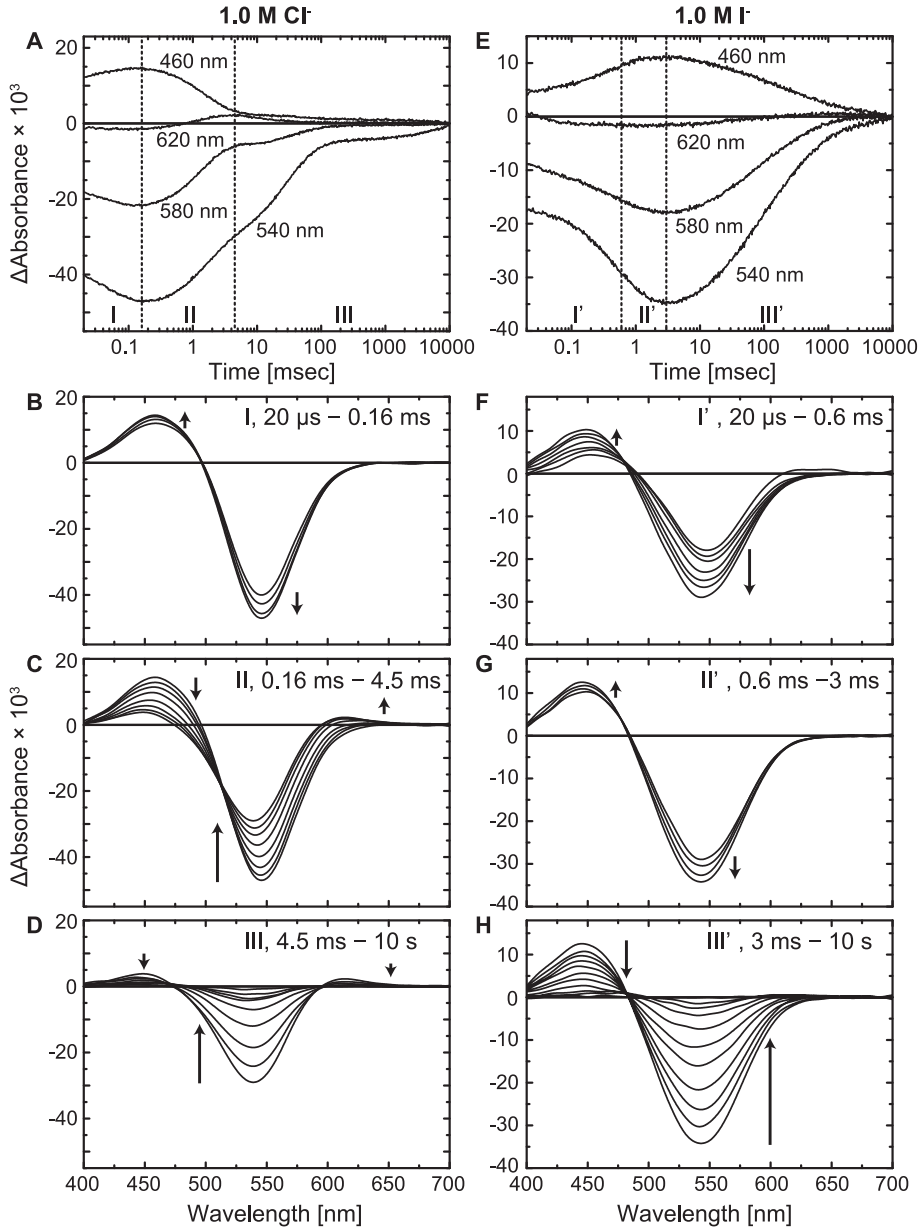

Fig. 2. Comparison of flash-induced absorbance changes between the Cl^-- and I^--bound MrHR. The buffer solution was 10 mM MOPS, pH 6.5, containing 0.1% DDM, 1.0 M Na_2SO_4 and 1.0 M NaCl (left column) or 1.0 M NaI (right column). Top panels are the time courses of flash-induced absorbance changes at characteristic wavelengths. Lower panels are the light-dark difference spectra divided into three-time regions (I–III and I′–III′), which are indicated in the top panels with broken lines.

further. This band corresponds to L. Similar absorbance changes also appear in the time regions I′ and II′ for the I^--bound form. Their changes are slow, and thus, time region I for the Cl^--bound form (Panels A and B) approximately corresponds to region II′ for the I^--bound form (Panels E and G). Aside from the rate difference, the light-dark difference spectra in Panel G (time region II′) are quite similar to those in Panel B (time region I), suggesting that the photocycles until the L formations are essentially the same between the Cl^--bound and I^--bound forms. However, their subsequent photocycles are quite different. For the Cl^--bound form, the L decay leads to O formation at approximately 620 nm (Panels A and C). As shown here, O formation is completed at the end of region II (~4.5 ms). Even at that time, a positive absorbance change at 460 nm still remains. Thus, O probably forms a quasi-equilibrium with an L-like intermediate. In a previous report, we tentatively named this intermediate N after the photocycle of NpHR, where O develops an equilibrium with N [19,22]. As shown in Panel A, the O decay is almost complete by 100 ms. After that, a small negative band at approximately 540 nm remains and then slowly decays (Panel A). This is the prolonged decay of the last intermediate MrHR′, which has almost the same spectrum as the dark state. On the other hand, the I^--bound form undergoes a simple photocycle. As shown in Panels E and H, the decay of the 460 nm band almost matches with the recovery of the 540 nm band. Thus, for the I^--bound form, L directly returns to the original dark state by not going through N and O. This implies that in the Cl^--pumping photocycle, Cl^- moves to the CP channel across the Schiff base region during the formation of the N and O mixture. However, in the I^--bound transport-disabled protein, I^- cannot cross the Schiff base region, and the photocycle cannot proceed after the L intermediate.

To examine the details of the Cl^--pumping photocycle, we analyzed the flash-induced absorbance changes according to the sequential irreversible model [21]. Here, we analyzed the data in the presence of

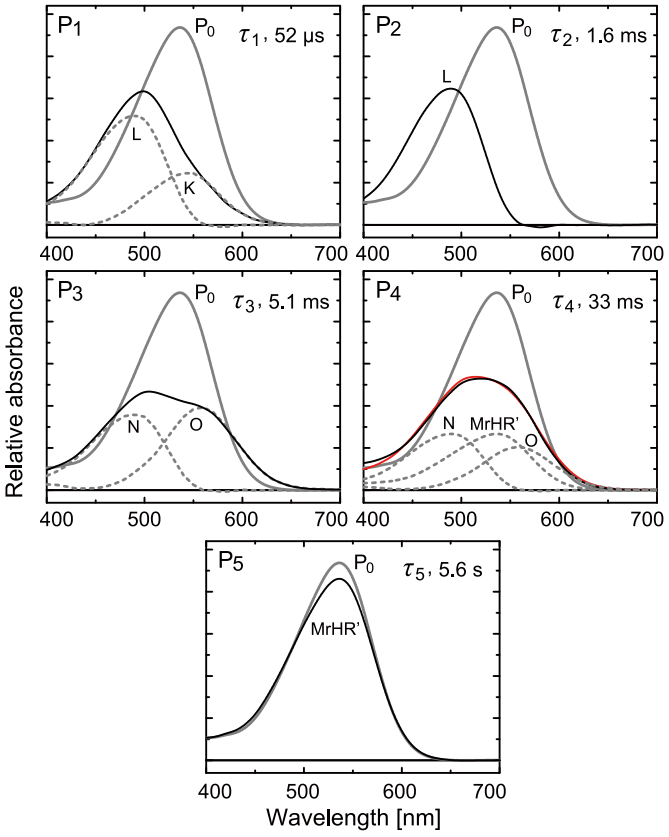

Fig. 3. Global fitting results of the flash photolysis data at 1 M Cl^-. The data in the left panels of Fig. 2 were analyzed according to the sequential irreversible model. Absorption spectra of P_1–P_5 states (black line) are shown with their decay time constants (τ_1–τ_5). P_0 indicates the unphotolyzed state. The spectra of the P_1, P_3 and P_4 states were decomposed into the spectra of the physically defined intermediates (gray broken lines). For P_4, the sum of the spectral components is also plotted with a red line.

100 mM to 4 M Cl^-, where the ionic strengths were kept constant at a value equivalent to 4 M NaCl by the addition of Na_2SO_4. For all datasets, the best fitting results were obtained with a five-exponential function, indicating the existence of five kinetically distinguishable states (P_i, i = 1–5). The final obtained P_i spectra in the presence of 1 M Cl^- are shown in Fig. 3 (black lines) together with their decay time constants and the spectrum of their unphotolyzed state (P_0, thick gray lines). Among the five P_i states, only P_2 and P_5 have narrow absorption spectra. Thus, they contain single physically defined intermediates. Judging from the λ_{max} (490 nm for P2 and 535 nm for P5) and the timing of their appearance, they are attributable to L and MrHR′, respectively. Other P_1, P_3 and P_4 states have broad spectra and thus contain the equilibrium of physically defined intermediates. Here, we tried to decompose those P_i spectra into the spectral components of the intermediates. The deduced spectra are shown in each panel with gray broken lines. The P_1 state has a λ_{max} similar to P_2 but also has a shoulder at approximately 550 nm. Thus, P_1 should be the equilibrium between L and its precursor K. The deduced L spectral component was calculated from the P_2 spectrum by multiplying it by 0.8. The K component was calculated by subtraction of the L component from the P_1 spectrum. The resultant K spectrum has a λ_{max} at approximately 545 nm. Similar to P_1, P_3 contains shorter and longer wavelength intermediates attributable to N and O, respectively. Their spectral components were deduced by assuming that N has almost the same spectrum as L. The N component was calculated from P_2 by multiplying it by 0.55. The O component was calculated by subtraction of the N component from the P_3 spectrum. The resultant O spectrum has a λ_{max} at approximately 560 nm. The subsequent P_4 could not be described by the sum of N and O. It needs an additional contribution of MrHR′, which solely appears in the P_5 state. The sum of the three deduced components (N, O and MrHR′) is shown by a red line, which effectively simulates the P_4 spectrum. The MrHR′ component was calculated from P_5 by multiplying it by 0.31. The N and O components were calculated from those in P_3 by multiplying them by 0.75 and 0.53, respectively. The larger coefficient for N between these two suggests that N might arise from O and decay to MrHR′. Thus, the tentative photocycle scheme could be described as: $MrHR_{537} \rightarrow K_{545} \leftrightarrow L_{490} \rightarrow O_{560} \leftrightarrow N_{490} \leftrightarrow MrHR'_{535} \rightarrow MrHR_{537}$. As described above, the Cl^- probably moves to the CP channel during L decay. For NpHR, O arises from N and decays to NpHR′ [19]. The order of N and O together with the molecular difference between L and N should be clarified in future investigations.

Here, we employed DDM-solubilized MrHR. The solubilization was reported to affect the photocycle of MrHR, especially to prolong the decay of MrHR′ [32]. However, the overall photocycle is essentially the same as that of MrHR embedded in the lipid membrane. As shown in Fig. S1, the solubilized MrHR did not show a significant Cl^- concentration dependence in both of the P_i spectra and their decay time constants. Thus, we could not discuss the details of the Cl^- release and reuptake processes. In contrast, a distinct Cl^- concentration dependence was reported for the MrHR photocycle embedded in the lipid membrane [32]. However, this dependence might also reflect differences in the ionic strength. As shown in Fig. S2A, the photocycle shows a distinct Cl^- concentration dependence when we added only NaCl into the medium. However, this modification became small when we retained the ionic strength by supplementing it with Na_2SO_4 (Panel B). Thus, further study is needed to clarify the Cl^- dependence of the MrHR photocycle.

3.2. Mutational analyses of MrHR

We replaced several amino acid residues to identify the important ones for MrHR function. The mutated residues are shown in Fig. 1, including (i) three motif residues (Thr74, Ser78, Asp85), (ii) superconserved residues among microbial rhodopsins (Arg71, Asp200), and (iii) two Glu residues (Glu182, Glu192), which are also conserved in BR as H^+ releasing complex.

3.2.1. Cl^--induced spectral shift

As described above, unphotolyzed MrHR already binds Cl^- in the vicinity of the protonated Schiff base. This binding induces an absorption spectral shift like other Cl^- pumps [12]. However, the shift direction is opposite to most Cl^- pumps, which show a Cl^--induced blueshift [31,33,34]. Only one exception was reported for HR from *H. salinarum* (HsHR), where an approximate 10 nm redshift was observed [35–37]. However, this observation might include the effect of rapid dark adaptation at a low Cl^- concentration. In our previous experiment where the light-adapted HsHR was prepared at all Cl^- concentrations, we observed only an increase in the extinction coefficient without the spectral shift [17]. Meanwhile, MrHR does not show the light/dark adaptation itself [12]. Thus, the distinct redshift is probably a unique feature of MrHR, which might reflect specific differences around the Cl^--binding site from other Cl^- pumps.

As shown in Fig. 4A–H, most mutants showed a redshift similar to the wild-type MrHR. However, two mutants of T74A (C) and E182Q (F) showed an opposite blueshift. As discussed later, these results might be related to the protonation state of Asp200 residue corresponding to Asp212 of BR (Fig. 1). To determine the K_d values of Cl^-, the absorbance changes (ΔA) at λ_{max} after Cl^- bindings were fitted by Eq. (1). In Fig. 4I, the relative ΔA were plotted. The determined K_d and n values are listed in Table 1. Other three parameters, $\lambda_{max,0}$, $\lambda_{max,\ Cl^-}$, and $\Delta\lambda_{max}$ in Table 1 were determined by the analyses with Eq. (2). Those fitting curves are shown in Fig. S3 and the determined parameters are listed in Table S1. The wild-type MrHR binds Cl^- with a K_d of

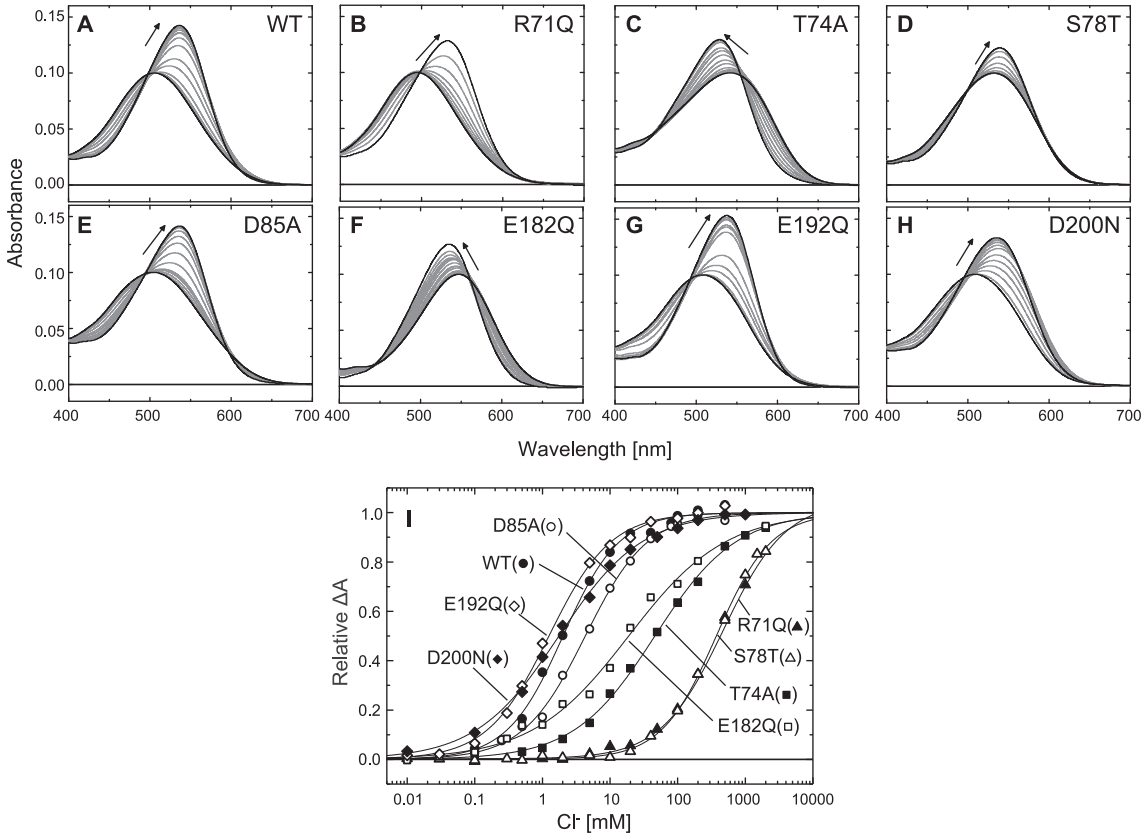

Fig. 4. Cl^--induced absorption spectral shifts of the wild-type MrHR (A) and the mutants (B–H). The medium contained 10 mM MOPS (pH 6.5), 33 mM Na_2SO_4, 0.1% DDM and NaCl (0–2.0 M). The shift directions are indicated with black arrows. The absorbance changes at λ_{max} after Cl^--bindings (ΔA) were fitted with Eq. (1) to determine the K_d values. In Panel I, the relative ΔA are plotted. The fitting results are summarized in Table 1.

Table 1
Fitting parameters for the Cl^--induced absorption spectral shifts of the wild-type MrHR and the mutants.

	K_d [mM][a]	n[b]	$\lambda_{max,0}$ [nm][c]	$\lambda_{max,\ Cl^-}$ [nm][d]	$\Delta\lambda_{max}$ [nm][e]
WT	2.02 ± 0.16	1.05 ± 0.07	506	537	+31
R71Q	385 ± 14	0.96 ± 0.03	495	532	+37
T74A	46.0 ± 3.8	0.73 ± 0.04	542	529	−13
S78T	373 ± 26	1.07 ± 0.05	533	539	+6
D85A	4.31 ± 0.24	0.94 ± 0.05	506	536	+30
E182Q	18.9 ± 3.5	0.61 ± 0.06	547	535	−12
E192Q	1.25 ± 0.09	0.95 ± 0.05	509	537	+28
D200N	1.76 ± 0.13	0.71 ± 0.04	507	537	+30

[a,b] K_d and n were determined by the fitting analyses with Eq. (1). Here, we fitted the Cl^--induced absorbance changes at respective $\lambda_{max,\ Cl^-}$, whose values are also listed in the table.
[c,d,e] $\lambda_{max,0}$, $\lambda_{max,\ Cl^-}$ and $\Delta\lambda_{max}$ denote the λ_{max} values in the Cl^--free states, Cl^--bound states, and their differences, respectively. They were determined by the fitting analyses with Eq. (2). The fitting curves are shown in Fig. S3 and all determined parameters are listed in Table S1.

approximately 2 mM. This affinity was greatly weakened in R71Q (385 mM) and S78T (373 mM) and moderately in T74A (46.0 mM) and E182Q (18.9 mM). These four residues are also conserved in HR (Fig. 1), where the former three residues are close to the bound Cl^- [38,39]; in particular, the former two residues (Arg and Ser) are also known to provide significant contributions to the Cl^- binding [40–42]. Thus, the residues consisting of Cl^--binding sites are common with HR. However, notable differences exist in the significance of the Arg residue. For MrHR, R71Q still maintains its Cl^--binding affinity and its Cl^--pumping activity, as described below. However, the corresponding HR mutants (R123Q for NpHR, R108Q for HsHR) completely lose their affinity and thus lose their Cl^--pumping activity [40,42]. The Arg residue in HR faces toward the Cl^- binding site [38,39]. The direction of this Arg might be different in MrHR, similar to other microbial rhodopsins such as SRII [43], *Anabaena* sensory rhodopsin [44], xanthorhodopsin [45], and channelrhodopsin [46], in which the Arg residue faces toward the EC side. The lesser significance of Arg might be accountable for the different direction. The fourth residue Glu182 is probably located around the EC surface, as shown in Fig. 1. Nevertheless, the E to Q mutation weakens the Cl^- binding affinity by approximately 10 times, indicating that the Glu182 residue is deprotonated and has a long-range interaction with the Cl^--binding site. For NpHR, the corresponding mutant E234Q also showed a Cl^--binding affinity 10 times weaker than that of the wild-type NpHR (our unpublished result). Thus, this long-range interaction might also be common for MrHR and HR. Another Glu residue, Glu192, is probably located near Glu182. However, the E192Q mutation did not affect the Cl^--binding affinity, implying that this residue might be protonated, unlike the Glu182 residue.

In addition to E192Q, D85A and D200N affected neither the Cl^--binding affinity nor the λ_{max} before or after the Cl^--binding. The negligible effects of D85A probably reflect the hydrophobic environment surrounding this residue. In many microbial rhodopsins, the hydrophobic CP channel is isolated along with the Schiff base region from their hydrophilic EC channel. However, the negligible effects of D200N seem notable. Asp200 is located in the vicinity of the protonated Schiff base and is superconserved among the microbial rhodopsins. Their Asp residues are considered to be deprotonated due to their low pKas. For the Asp238 of HsHR, the estimated pKas are −2.0 for the Cl^--free form and 4.8 for the Cl^--bound form [38], indicating that this residue is deprotonated regardless of the Cl^- binding. Moreover, the theoretical

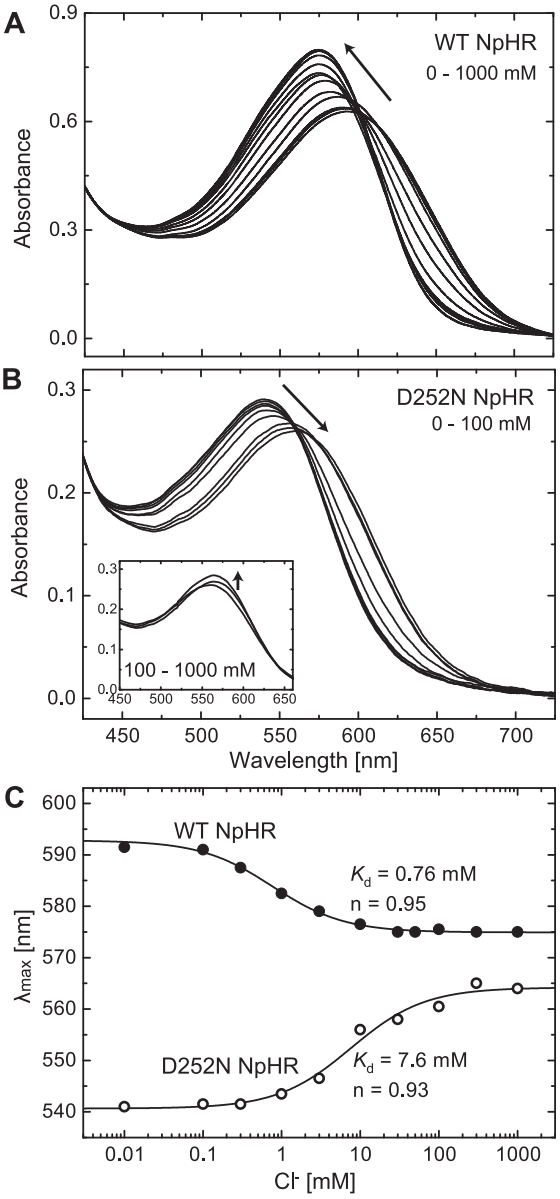

Fig. 5. Cl^--induced absorption spectral shifts of the wild-type NpHR (A) and the D252N mutant (B). The membrane fragments prepared from *H. salinarum* cells were used for the samples. The medium contained 10 mM MES (pH 6.5), 1.5 M Na_2SO_4 and NaCl (0–1.0 M). The shift directions are indicated with black arrows. The Cl^- dependences of the λ_{max} are plotted in Panel C. They were fitted with Eq. (2) to determine the K_d. The fitting results are also indicated in the panel.

calculations (DFT-QM/MM) predict the significant redshift of λ_{max} upon protonation of the Asp238 residue [47]. For Asp212 of BR, the pKa is approximately 1 [48]. Reflecting this deprotonated state, the D to N mutation (D212N) results in a 17 nm redshift of λ_{max} [49]. A significant influence of the deprotonated Asp residue is also reported for SRII from *Natronomonas pharaonis* based on the QM/MM calculations [50]. Thus, the negligible effect of D200N MrHR might indicate that this residue in the wild type is protonated regardless of Cl^- binding.

For other Cl^- pumps, the spectral features of mutants corresponding to D200N MrHR have not been previously reported. Thus, we made the D252N NpHR and examined this mutation's effects. Here, we employed the *H. salinarum* strain Pho81Wr$^-$ [18], because D252N was not functionally expressed in the *E. coli* membrane. Fig. 5A and B show the Cl^--induced spectral shifts of wild-type NpHR and its D252N mutant, respectively. Their λ_{max} are plotted against the Cl^- concentration in Fig. 5C. In contrast to MrHR, the D252N mutation has significant impacts on NpHR. A notable difference appears in the spectral shift direction. As shown in Panel A, the wild-type NpHR shows a Cl^--induced blueshift similar to other Cl^- pumps. However, D252N NpHR shows a redshift (Panel B). Namely, this is the same direction as the wild-type MrHR and its D200N mutant. Moreover, the D252N mutation significantly affects the λ_{max} in both the Cl^--free and the Cl^--bound forms (Panel C). In the Cl^--free form, this mutation induced a 52 nm blueshift (593 nm → 541 nm). Upon Cl^- binding, this shift became small (11 nm) but still distinct (575 nm → 564 nm). The dissociation constant of Cl^- was also affected: the D252N mutation weakened the Cl^--binding affinity by approximately 10 times (0.76 mM → 7.6 mM). Similar dissociation constants were also obtained from the analyses of absorbance changes (Fig. S4 and Table S1). These results are in accordance with the presumption that Asp200 of MrHR maintains a protonated state before and after the Cl^- binding.

For D252N NpHR, the addition of Cl^- over 100 mM induced a further spectral change (inset of Panel B): the extinction coefficient slightly increased without a spectral shift. This lesser effect might reflect the binding of another Cl^-, but its location is probably far from the chromophore. For MrHR, a similar increase in the extinction coefficient was not observed.

As mentioned above, T74A and E182Q mutants showed a Cl^--induced blueshift, which is in the opposite direction of the wild-type MrHR. This infers that these mutants might involve the deprotonated Asp200 residue similar to NpHR. However, as described later, we observed a light-induced H^+ transfer reaction (Fig. 7, lower thin panels), which is probably released from Asp200, for both of these mutants and the wild type, suggesting that their Asp200 are protonated in the Cl^--binding states. Thus, these mutants probably follow a rather complicated scenario: in the Cl^--free form, their Asp200 might be deprotonated, while upon Cl^- binding, it becomes protonated.

3.2.2. Cl^--pumping activities and photocycles

For the activity measurements, we used the *E. coli* cells expressing MrHR and a conventional pH electrode system. Upon light irradiation, the cell suspension was alkalized due to the passive proton influx in response to the inward Cl^- transport by MrHR. Fig. 6A shows the time-dependent pH changes under illumination. Their magnitudes should depend on the MrHR expression levels, which were estimated by flash-induced absorbance changes at the respective λ_{max}. The relative pumping activities are shown in Panel B, where the initial slopes of light-induced pH changes (Panel A) are plotted after dividing them by the relative expression levels (Panel C). The most intensive effect on the activity was observed in D200N MrHR (Panel A and B). All other mutants maintained their distinct Cl^- pumping activities, whereas the activity completely disappeared in the D200N mutant. As described above, the Asp200 residue is probably protonated in the dark state. Thus, upon photoexcitation, this residue might deprotonate and then drives the Cl^- translocation. A complete loss of activity was also reported for D252N NpHR [51], the corresponding mutant to D200N MrHR. Thus, a negative charge at this position is essential for both Cl^- pumps. However, the Asp252 residue of NpHR is already deprotonated in the dark state.

Interestingly, the E182Q mutant showed higher activity than the wild type. This unexpected result will be discussed later. Meanwhile, three mutants of T74A, S78T and E192Q show significantly weakened activities. The former two have lower Cl^--binding affinities, whereas the latter one has an affinity comparable to the wild type. Thus, the lower affinity is not the cause of the weaker activity. Indeed, the R71Q mutant, which has the weakest Cl^--binding affinity, exerts a relatively higher activity. As described later, these three mutants and R71Q undergo essentially the same photocycle as the wild type. Thus, the present results could not explain their lower activity. A detailed analysis of their photocycle should be performed in a future investigation.

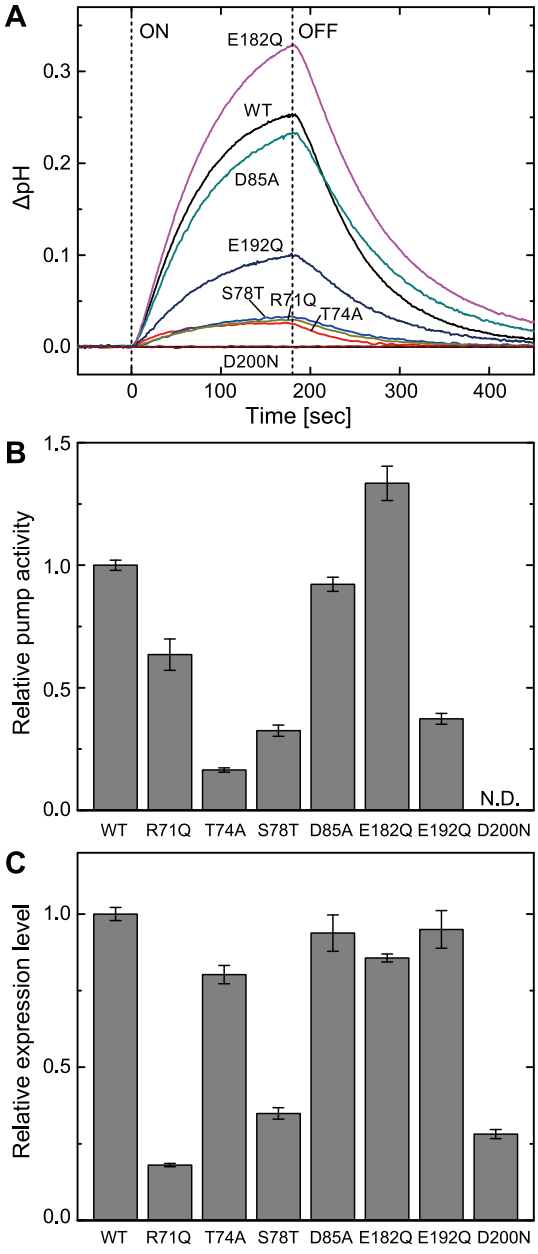

Fig. 6. Cl^--pumping activities of the wild-type MrHR and the mutants. The light-induced pH changes were measured for the suspensions of *E. coli* cells expressing MrHR. Their time courses are shown in Panel A. The relative pumping activities in Panel B were calculated from the initial slopes of the pH changes and the relative expression amounts of the proteins in Panel C (see text for details). For D200N, activity was not detected (N.D.). Each bar represents mean ± SD (n = 3–4). The medium contained 200 mM NaCl and 10 μM CCCP. The initial pH values were approximately 6.0–6.5.

The flash photolysis data are shown in the large panels of Fig. 7. Here, we also plotted the data for the wild type in the Cl^-- and I^--bound forms (Panels A and B). Most data were obtained at 0.1 M halide ions (Cl^- or I^-), whereas the data for R71Q, T74A and S78T (Panels C-D) were obtained at 4 M Cl^- due to their weak Cl^--binding affinity. For the wild type (Panels A and B), significant differences between the Cl^--bound and I^--bound forms appeared to be similar to the data in Fig. 2 that were obtained at 1 M Cl^- and 1 M I^-, respectively. For the I^--bound form (Panel B), the signals at 460 nm and 540 nm decayed simultaneously, but for the Cl^--bound form (Panel A), the 460 nm signal decayed faster than the 540 nm signal due to the formation of the N and O mixture. As shown in Panels C–H, most mutants undergo photocycles that are essentially the same as the Cl^--bound form of the wild type. In contrast, only the D200N mutant (Panel I) shows a photocycle similar to the I^--bound form of the wild type, even though this mutant binds Cl^- in the dark state. Thus, D200N MrHR probably cannot move Cl^- to the CP channel during L decay similar to the I^--bound form of the wild type.

Most data in Fig. 7 were obtained at pH 6.5, which is close to the measured pH of 6.0–6.5 for the Cl^--pumping activities (Fig. 6). However, the data for D200N (Fig. 7I) were obtained at pH 5.0. At pH 6.5, this mutant undergoes a different photocycle (Fig. S5A), where a short wavelength intermediate appears at 400 nm after L decay (460 nm). This intermediate probably reflects the deprotonated Schiff base similar to the M intermediate of the H^+-pumping rhodopsins. However, this deprotonation is not the reason for the lack of pumping activity. The D200N mutant still did not show any pumping activity at around pH 5 (data not shown), where M does not appear in the photocycle (Fig. 7I). As discussed later, the deprotonation of the Schiff base might be caused by the lack of prior deprotonation of the Asp200 residue. Thus, in Fig. 7I, the data at pH 5 are plotted for comparison with other photocycles.

3.2.3. H^+-transfer reactions

The microbial rhodopsins have common features in two half channels: their CP channels are closed and hydrophobic, while the EC channels are commonly open and hydrophilic. The Asp200 residue of MrHR should be located in the EC channel, and thus, the H^+ from this residue might be released into the medium though the EC channel. Thus, we tried to detect this H^+ release by using an ITO electrode. The results are shown in the thin panels of Fig. 7. The upward shift of the voltage indicates H^+ release from the protein, whereas the downward shift indicates H^+ uptake by the protein. As shown in Panel A, the Cl^--bound form of the wild-type MrHR causes distinct H^+ transfer reactions, where the H^+ release occurs first and is followed by uptake. The H^+ release occurs almost simultaneously with L decay, whereas the H^+ uptake occurs after the decay of the N and O mixture. For most of the mutants (Panels C–H), similar H^+ transfer reactions were observed. In contrast, the H^+ transfer reactions disappeared in the D200N mutant (Panel I). This suggests that, in the Cl^--pumping photocycle, the Asp200 residue directly releases H^+ into the medium. Interestingly, the I^--bound form of the wild type (Panel B) also lacks H^+ transfer reactions. In the I^--bound form, the Asp200 residue probably does not deprotonate, and thus, I^- cannot move into the CP channel. A previous FTIR study revealed the deprotonation of the Asp85 residue during the photocycle [32]. However, the H^+ release signal was still observed in the D85A mutant (Panel F). Thus, the Asp85 residue is not the origin of the released H^+.

For D200N, we plotted the ITO data at pH 5.0 similar to its flash photolysis data. At pH 6.5, D200N shows a distinct H^+ transfer signal, as shown in Fig. S5A. However, its time course almost matches the formation and decay of M (400 nm). Thus, this H^+ release probably reflects the deprotonation of the Schiff base. Even at pH 5, the wild type and other mutants showed essentially the same photocycles with those at pH 6.5. The data for the wild type are shown in Fig. S5B and C. Even at pH 5.0, the Cl^--bound form still shows an H^+ transfer signal, but its I^--bound form lacks this signal.

For these measurements, we made the lipidic films on the ITO surface. Probably, ITO mainly senses the H^+ from MrHR near the film surface but hardly senses the H^+ from embedded MrHR due to the barrier effect of the surrounding membranes. Thus, the signal magnitude does not reflect the total amount of H^+ from MrHR. However, we could compare the magnitudes among the samples, because all films were made with the same amounts of lipid and MrHR. Thus, the barrier effect should be almost the same among the samples. The R71Q, S78T and D85A showed smaller signals. The R71Q and S78T have weak Cl^--binding affinities in the dark states, whereas all ITO measurements were performed at 0.1 M Cl^-. Thus, the smaller magnitudes probably

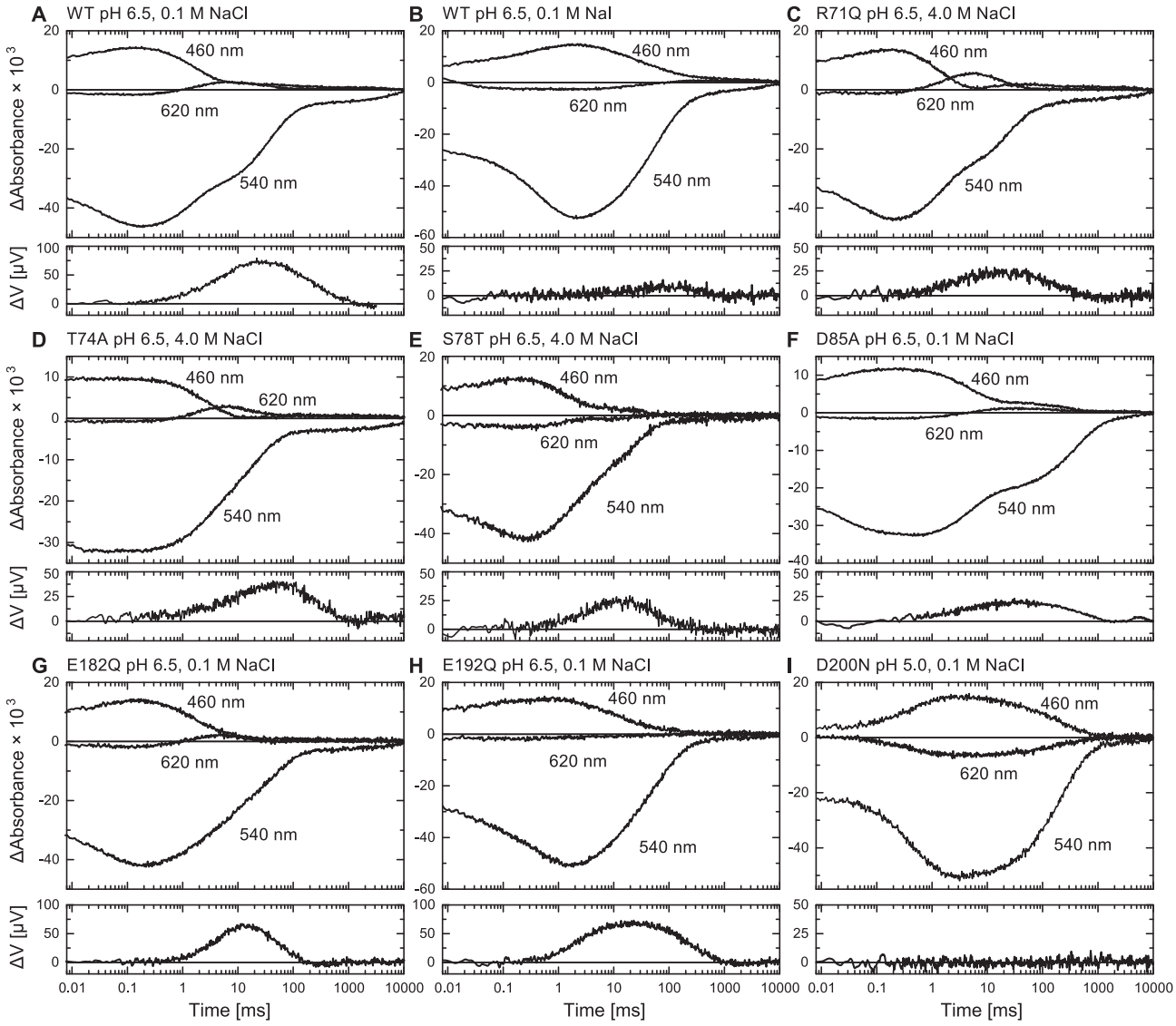

Fig. 7. Photocycles of the wild-type MrHR and the mutants. Flash-induced absorbance changes at selective wavelengths (large panels) are shown together with the H^+ transfers measured using an ITO electrode (thin panels). The mediums were 6-mix buffer containing NaCl or NaI. The pH values and the salt concentrations for flash photolysis are indicated above the respective panels. All ITO data were taken with 0.1 M salt, while the pH values were the same as those for the flash photolysis data. The mediums for flash photolysis were supplemented with 0.1% DDM.

reflect the lesser amount of proteins undergoing the Cl^--pumping photocycle. For D85A, its Cl^--binding affinity is comparable with the wild type, but smaller ITO signal was observed. This discrepancy might relate with its slower L decay. As discussed above, MrHR probably releases H^+ during the L decay. Thus, slower L decay could reduce the accumulation of the released H^+. For T74A, the Cl^--binding affinity is relatively weak, whereas for E192Q, it is comparable with the wild type. Corresponding to these affinities, the ITO signal is relatively weak for T74A but strong for E192Q. Interestingly, E182Q seems to violate this rule. The E182Q has relatively weak Cl^--binding affinity but showed strong ITO signal. As discussed above, the E182 residue of the wild type is probably deprotonated in the dark state. This negative charge might reduce the H^+ released to the medium. Due to the lack of the negative charge, the E182Q might have higher H^+-releasing efficiency, which might compensate the relatively weak Cl^--binding affinity.

The negative charge at 182nd position also seems to affect the H^+-uptake rate. For the wild type and most mutants, the H^+ uptake does not match with the decay of N and O mixture at 620 nm, corresponding to the formation of MrHR′ at 540 nm. Their H^+ uptakes occur after these transitions, whereas for E182Q, its H^+ uptake almost matches with these transitions, indicating that the removal of the negative charge at 182nd position accelerates the H^+ uptake. However, the lack of negative charge seems to rather decelerate the H^+ uptake. Thus, the faster H^+ uptake might reflect the altered structure: The removal of the negative charge might induce rather opened structure of the EC channel, which might facilitate the H^+-transfer reaction. The E182Q mutant is also unique regarding the Cl^--pumping activity as mentioned above: This mutant shows higher pumping activity than the wild type (Fig. 6B). The activity difference could not be explained by the turnover rate, because they showed almost the same photocycling rate (Fig. 7A and G). One possible explanation might be the photoreactivity of MrHR′ after H^+ uptake. During the formation of MrHR′, this protein probably binds new Cl^- near the original position. Upon subsequent H^+ uptake, MrHR′ might become photoreactive and ready to go the next photocycle. In this case, the faster H^+ uptake of E182Q could contribute to the higher turnover rate. This two-photon process should be examined in the future investigation.

3.3. The transient deprotonation of the Asp200 residue

This residue is superconserved in microbial rhodopsins. By analogy with BR and HR [38,48], the corresponding Asp residues seem to be deprotonated at both photolyzed and unphotolyzed states due to their low pKas. Thus, the protonated state of Asp200 in the dark might be a unique feature of MrHR. To determine the pKa of this residue, we tried to detect its deprotonation by means of the pH-induced λ_{max} shift. However, we did not observe a distinct shift before the deprotonation of the Schiff base. Thus, the pKa is probably higher than that of the Schiff base, whose value is approximately 9.4. The Cl^- binding might influence the pKa of Asp200. However, this residue is probably protonated even in the Cl^- free state, as described above. In BR, the low pKa of Asp212 is achieved by complex interactions, such as hydrogen bonding interactions with Tyr57, Tyr185 and water molecules [52] and electrostatic interactions with Arg82 [53]. These residues are also conserved in MrHR, but the locations of their side chains might be different from those in BR. The resultant hydrophobic environment might enforce the protonation of Asp200.

During the photocycle, Asp200 probably deprotonates and then drives the Cl^- movement to the CP channel. Light-induced deprotonation is probably caused by a conformational change, which might enable Asp200 to interact with hydrophilic residues and/or water molecules. In addition to these interactions, the protonated Schiff base might also be involved in this reaction. As mentioned above, the Schiff base of the D200N mutant deprotonates during the photocycle at pH 6.5. This implies that the Schiff base has a lower pKa in the photolyzed state. The lowered pKa should involve the localization of a positive charge in the NH^+ region, which might induce the deprotonation of Asp200. The resulting negative charge could not only drive the Cl^- movement but also prevent the deprotonation of the Schiff base. In the photocycle of D200N mutant, the Schiff base takes a lower pKa, but the negative charge is not formed at the 200th position. This results in no Cl^- movement in addition to the deprotonation of the Schiff base, although the latter occurs only above pH 6. For the I^--bound form of the wild type, the pKa of the Schiff base might not decrease due to some reasons. This should cause the lack of the three reactions involved in the deprotonation of the D200 residue, the resultant movement of I^-, and the deprotonation of the Schiff base.

4. Conclusions

In this study, we obtained the following findings regarding the photoreaction of MrHR: 1) the photolyzed MrHR moves Cl^- to the CP channel during L decay, 2) this Cl^- movement requires a negative charge at the 200th position, and 3) the Asp200 residue is probably protonated but deprotonates during L decay to create this negative charge. For the protonation state of Asp200, additional convincing evidence such as FTIR should be used in future investigations. The negative charge corresponding to the 200th position is also essential for NpHR [51] and probably for other Cl^- pumps. As mentioned above, MrHR probably developed from the ancient BR-type H^+ pump, but it does not seem to be fully optimized like other Cl^- pumps. This Asp residue might be one of the optimized residues in other Cl^- pumps, in which the Asp residues always maintain their deprotonated state. What is the benefit of this optimization? For MrHR, the H^+ from the Asp200 residue is probably released into the EC medium. The resultant dipole moment might hamper the opposite movement of Cl^- into the CP channel and then weaken the Cl^--pumping activity. Thus, the other Cl^- pumps might be optimized so that they can bind Cl^- with high affinity and then transport it, even though the Asp residues are always deprotonated.

Transparency document

The Transparency document associated with this article can be found, in online version.

Acknowledgements

We thank Prof. John L. Spudich at the University of Texas-Houston Medical School for providing the pJS010 plasmid and Pho81Wr$^-$ strain, and Hiroaki Ichio for his help in absorption spectra measurements. This work was supported by JSPS KAKENHI granted to T.K. (17K07326) and M.D. (16K14044). This research was also supported by the Global Station for Soft Matter, a project of the Global Institution for Collaborative Research and Education at Hokkaido University.

Appendix A. Supplementary data

Supplementary data to this article can be found online at https://doi.org/10.1016/j.bbabio.2018.12.001.

References

[1] O.P. Ernst, D.T. Lodowski, M. Elstner, P. Hegemann, L.S. Brown, H. Kandori, Microbial and animal rhodopsins: structures, functions, and molecular mechanisms, Chem. Rev. 114 (2014) 126–163.
[2] J.L. Spudich, O.A. Sineshchekov, E.G. Govorunova, Mechanism divergence in microbial rhodopsins, Biochim. Biophys. Acta 1837 (2014) 546–552.
[3] D. Oesterhelt, W. Stoeckenius, Rhodopsin-like protein from the purple membrane of *Halobacterium halobium*, Nature 233 (1971) 149–152.
[4] A. Matsuno-Yagi, Y. Mukohata, Two possible roles of bacteriorhodopsin; a comparative study of strains of *Halobacterium halobium* differing in pigmentation, Biochem. Biophys. Res. Commun. 78 (1977) 237–243.
[5] B. Schobert, J.K. Lanyi, Halorhodopsin is a light-driven chloride pump, J. Biol. Chem. 257 (1982) 10306–10313.
[6] D. Oesterhelt, W. Stoeckenius, Functions of a new photoreceptor membrane, Proc. Natl. Acad. Sci. U. S. A. 70 (1973) 2853–2857.
[7] A. Matsuno-Yagi, Y. Mukohata, ATP synthesis linked to light-dependent proton uptake in a red mutant strain of *Halobacterium* lacking bacteriorhodopsin, Arch. Biochem. Biophys. 199 (1980) 297–303.
[8] D. Oesterhelt, Structure and function of halorhodopsin, Isr. J. Chem. 35 (1995) 475–494.
[9] O. Béjà, L. Aravind, E.V. Koonin, M.T. Suzuki, A. Hadd, L.P. Nguyen, S.B. Jovanovich, C.M. Gates, R.A. Feldman, J.L. Spudich, E.N. Spudich, E.F. DeLong, Bacterial rhodopsin: evidence for a new type of phototrophy in the sea, Science 289 (2000) 1902–1906.
[10] K. Inoue, H. Ono, R. Abe-Yoshizumi, S. Yoshizawa, H. Ito, K. Kogure, H. Kandori, A light-driven sodium ion pump in marine bacteria, Nat. Commun. 4 (2013) 1678.
[11] S. Yoshizawa, Y. Kumagai, H. Kim, Y. Ogura, T. Hayashi, W. Iwasaki, E.F. DeLong, K. Kogure, Functional characterization of flavobacteria rhodopsins reveals a unique class of light-driven chloride pump in bacteria, Proc. Natl. Acad. Sci. U. S. A. 111 (2014) 6732–6737.
[12] T. Hasemi, T. Kikukawa, N. Kamo, M. Demura, Characterization of a cyanobacterial chloride-pumping rhodopsin and its conversion into a proton pump, J. Biol. Chem. 291 (2016) 355–362.
[13] A. Niho, S. Yoshizawa, T. Tsukamoto, M. Kurihara, S. Tahara, Y. Nakajima, M. Mizuno, H. Kuramochi, T. Tahara, Y. Mizutani, Y. Sudo, Demonstration of a light-driven SO_4^{2-} transporter and its spectroscopic characteristics, J. Am. Chem. Soc. 139 (2017) 4376–4389.
[14] T. Lazarova, C. Sanz, E. Querol, E. Padrós, Fourier transform infrared evidence for early deprotonation of Asp85 at alkaline pH in the photocycle of bacteriorhodopsin mutants containing E194Q, Biophys. J. 78 (2000) 2022–2030.
[15] S.P. Balashov, Protonation reactions and their coupling in bacteriorhodopsin, Biochim. Biophys. Acta 1460 (2000) 75–94.
[16] M. Sato, T. Kanamori, N. Kamo, M. Demura, K. Nitta, Stopped-flow analysis on anion binding to blue-form halorhodopsin from *Natronobacterium pharaonis*: comparison with the anion-uptake process during the photocycle, Biochemistry 41 (2002) 2452–2458.
[17] Y. Yamashita, T. Kikukawa, T. Tsukamoto, M. Kamiya, T. Aizawa, K. Kawano, S. Miyauchi, N. Kamo, M. Demura, Expression of salinarum halorhodopsin in *Escherichia coli* cells: solubilization in the presence of retinal yields the natural state, Biochim. Biophys. Acta 1808 (2011) 2905–2912.
[18] B. Perazzona, E.N. Spudich, J.L. Spudich, Deletion mapping of the sites on the HtrI transducer for sensory rhodopsin I interaction, J. Bacteriol. 178 (1996) 6475–6478.
[19] T. Kikukawa, C. Kusakabe, A. Kokubo, T. Tsukamoto, M. Kamiya, T. Aizawa, K. Ihara, N. Kamo, M. Demura, Probing the Cl^--pumping photocycle of pharaonis halorhodopsin: examinations with bacterioruberin, an intrinsic dye, and membrane potential-induced modulation of the photocycle, Biochim. Biophys. Acta 1847 (2015) 748–758.
[20] T. Kikukawa, C.K. Saha, S.P. Balashov, E.S. Imasheva, D. Zaslavsky, R.B. Gennis, T. Abe, N. Kamo, The lifetimes of pharaonis phoborhodopsin signaling states depend on the rates of proton transfers - effects of hydrostatic pressure and stopped flow experiments, Photochem. Photobiol. 84 (2008) 880–888.
[21] I. Chizhov, D.S. Chernavskii, M. Engelhard, K.H. Mueller, B.V. Zubov, B. Hess,

Spectrally silent transitions in the bacteriorhodopsin photocycle, Biophys. J. 71 (1996) 2329–2345.
[22] C. Hasegawa, T. Kikukawa, S. Miyauchi, A. Seki, Y. Sudo, M. Kubo, M. Demura, N. Kamo, Interaction of the halobacterial transducer to a halorhodopsin mutant engineered so as to bind the transducer: Cl^- circulation within the extracellular channel, Photochem. Photobiol. 83 (2007) 293–302.
[23] F. Schneider, C. Grimm, P. Hegemann, Biophysics of channelrhodopsin, Annu. Rev. Biophys. 44 (2015) 167–186.
[24] T. Kouyama, K. Ihara, K. Maki, S.K. Chan, Three-step isomerization of the retinal chromophore during the anion pumping cycle of halorhodopsin, Biochemistry 57 (2018) 6013–6026.
[25] K. Inoue, S. Tahara, Y. Kato, S. Takeuchi, T. Tahara, H. Kandori, Spectroscopic study of proton-transfer mechanism of inward proton-pump rhodopsin, *Parvularcula oceani* xenorhodopsin, J. Phys. Chem. B 122 (2018) 6453–6461.
[26] J. Tamogami, T. Kikukawa, S. Miyauchi, E. Muneyuki, N. Kamo, A tin oxide transparent electrode provides the means for rapid time-resolved pH measurements: application to photoinduced proton transfer of bacteriorhodopsin and proteorhodopsin, Photochem. Photobiol. 85 (2009) 578–589.
[27] T. Kikukawa, K. Shimono, J. Tamogami, S. Miyauchi, S.Y. Kim, T. Kimura-Someya, M. Shirouzu, K.H. Jung, S. Yokoyama, N. Kamo, Photochemistry of *Acetabularia* rhodopsin II from a marine plant, *Acetabularia acetabulum*, Biochemistry 50 (2011) 8888–8898.
[28] S. Nakamura, T. Kikukawa, J. Tamogami, M. Kamiya, T. Aizawa, M.W. Hahn, K. Ihara, N. Kamo, M. Demura, Photochemical characterization of actinorhodopsin and its functional existence in the natural host, Biochim. Biophys. Acta 1857 (2016) 1900–1908.
[29] E. Bamberg, P. Hegemann, D. Oesteriielt, Reconstitution of the light-driven electrogenic ion pump halorhodopsin in black lipid membranes, Biochim. Biophys. Acta 773 (1984) 53–60.
[30] A. Seki, S. Miyauchi, S. Hayashi, T. Kikukawa, M. Kubo, M. Demura, V. Ganapathy, N. Kamo, Heterologous expression of pharaonis halorhodopsin in *Xenopus laevis* oocytes and electrophysiological characterization of its light-driven Cl^- pump activity, Biophys. J. 92 (2007) 2559–2569.
[31] K. Inoue, F.H. Koua, Y. Kato, R. Abe-Yoshizumi, H. Kandori, Spectroscopic study of a light-driven chloride ion pump from marine bacteria, J. Phys. Chem. B 118 (2014) 11190–11199.
[32] A. Harris, M. Saita, T. Resler, A. Hughes-Visentin, R. Maia, F. Pranga-Sellnau, A.N. Bondar, J. Heberle, L.S. Brown, Molecular details of the unique mechanism of chloride transport by a cyanobacterial rhodopsin, Phys. Chem. Chem. Phys. 20 (2017) 3184–3199.
[33] B. Scharf, M. Engelhard, Blue halorhodopsin from *Natronobacterium pharaonis*: wavelength regulation by anions, Biochemistry 33 (1994) 6387–6393.
[34] T. Tsukamoto, S. Yoshizawa, T. Kikukawa, M. Demura, Y. Sudo, Implications for the light-driven chloride ion transport mechanism of *Nonlabens marinus* rhodopsin 3 by its photochemical characteristics, J. Phys. Chem. B 121 (2017) 2027–2038.
[35] T. Ogurusu, A. Maeda, N. Sasaki, T. Yoshizawa, Light-induced reaction of halorhodopsin prepared under low salt conditions, J. Biochem. 90 (1981) 1267–1274.
[36] G. Váró, L. Zimányi, X. Fan, L. Sun, R. Needleman, J.K. Lanyi, Photocycle of halorhodopsin from *Halobacterium salinarium*, Biophys. J. 68 (1995) 2062–2072.
[37] R.A. Bogomolni, M.E. Taylor, W. Stoeckenius, Reconstitution of purified halorhodopsin, Proc. Natl. Acad. Sci. U. S. A. 81 (1984) 5408–5411.
[38] M. Kolbe, H. Besir, L.O. Essen, D. Oesterhelt, Structure of the light-driven chloride pump halorhodopsin at 1.8 Å resolution, Science 288 (2000) 1390–1396.
[39] T. Kouyama, S. Kanada, Y. Takeguchi, A. Narusawa, M. Murakami, K. Ihara, Crystal structure of the light-driven chloride pump halorhodopsin from *Natronomonas pharaonis*, J. Mol. Biol. 396 (2010) 564–579.
[40] M. Rüdiger, U. Haupts, K. Gerwert, D. Oesterhelt, Chemical reconstitution of a chloride pump inactivated by a single point mutation, EMBO J. 14 (1995) 1599–1606.
[41] M. Sato, T. Kikukawa, T. Araiso, H. Okita, K. Shimono, N. Kamo, M. Demura, K. Nitta, Ser-130 of *Natronobacterium pharaonis* halorhodopsin is important for the chloride binding, Biophys. Chem. 104 (2003) 209–216.
[42] M. Kubo, T. Kikukawa, S. Miyauchi, A. Seki, M. Kamiya, T. Aizawa, K. Kawano, N. Kamo, M. Demura, Role of Arg123 in light-driven anion pump mechanisms of pharaonis halorhodopsin, Photochem. Photobiol. 85 (2009) 547–555.
[43] H. Luecke, B. Schobert, J.K. Lanyi, E.N. Spudich, J.L. Spudich, Crystal structure of sensory rhodopsin II at 2.4 angstroms: insights into color tuning and transducer interaction, Science 293 (2001) 1499–1503.
[44] L. Vogeley, O.A. Sineshchekov, V.D. Trivedi, J. Sasaki, J.L. Spudich, H. Luecke, *Anabaena* sensory rhodopsin: a photochromic color sensor at 2.0 Å, Science 306 (2004) 1390–1393.
[45] H. Luecke, B. Schobert, J. Stagno, E.S. Imasheva, J.M. Wang, S.P. Balashov, J.K. Lanyi, Crystallographic structure of xanthorhodopsin, the light-driven proton pump with a dual chromophore, Proc. Natl. Acad. Sci. U. S. A. 105 (2008) 16561–16565.
[46] H.E. Kato, F. Zhang, O. Yizhar, C. Ramakrishnan, T. Nishizawa, K. Hirata, J. Ito, Y. Aita, T. Tsukazaki, S. Hayashi, P. Hegemann, A.D. Maturana, R. Ishitani, K. Deisseroth, O. Nureki, Crystal structure of the channelrhodopsin light-gated cation channel, Nature 482 (2012) 369–374.
[47] R. Pal, S. Sekharan, V.S. Batista, Spectral tuning in halorhodopsin: the chloride pump photoreceptor, J. Am. Chem. Soc. 135 (2013) 9624–9627.
[48] G. Metz, Asp85 is the only internal aspartic acid that gets protonated in the M intermediate and the purple-to-blue transition of bacteriorhodopsin A solid-state ^{13}C CP-MAS NMR investigation, FEBS Lett. 303 (1992) 237–241.
[49] R. Needleman, M. Chang, B. Ni, G. Varo, J. Fornes, S.H. White, J.K. Lanyi, Properties of $Asp^{212} \rightarrow Asn$ bacteriorhodopsin suggest that Asp^{212} and Asp^{85} both participate in a counterion and proton acceptor complex near the Schiff base, J. Biol. Chem. 266 (1991) 11478–11484.
[50] M. Hoffmann, M. Wanko, P. Strodel, P.H. König, T. Frauenheim, K. Schulten, W. Thiel, E. Tajkhorshid, M. Elstner, Color tuning in rhodopsins: the mechanism for the spectral shift between bacteriorhodopsin and sensory rhodopsin II, J. Am. Chem. Soc. 128 (2006) 10808–10818.
[51] X.R. Chen, Y.C. Huang, H.P. Yi, C.S. Yang, A unique light-driven proton transportation signal in halorhodopsin from *Natronomonas pharaonis*, Biophys. J. 111 (2016) 2600–2607.
[52] H. Luecke, B. Schobert, H.T. Richter, J.P. Cartailler, J.K. Lanyi, Structure of bacteriorhodopsin at 1.55 Å resolution, J. Mol. Biol. 291 (1999) 899–911.
[53] S.P. Balashov, R. Govindjee, E.S. Imasheva, S. Misra, T.G. Ebrey, Y. Feng, R.K. Crouch, D.R. Menick, The two pKa's of aspartate-85 and control of thermal isomerization and proton release in the arginine-82 to lysine mutant of bacteriorhodopsin, Biochemistry 34 (1995) 8820–8834.